換氣中인 畜舍의 熱浮力이 공기유동 및 온도분포에 미치는 영향

The Effect of Thermal Buoyancy on Air Flow and Temperature Distribution in a Slot-Ventilated Livestock Building

崔 弘 林*
H. L. Choi

摘 要

환기중인 실험축사내에서 가축의 현열과 환기공기의 온도차에 의한 熱浮力(thermal buoyancy)이 공기유동 및 온도분포에 미치는 영향을 究明하기 위하여 TEACH 컴퓨터프로그램(k-ε 난류모형 및 SIMPLE계열 Algorithm)을 Curvilinear Coordinates에 맞게 변형하였다. 계산한 축사내 공기유통 및 온도분포의 有意性 검증은 Boon(1978)의 실험결과를 이용하였다. 열부력의 크기에 따른 유동의 변화를 관찰하기 위하여 유입공기의 온도를 17℃와 10℃ 두 수준으로 입력하였으며, 가축의 현열플럭스(flux)는 실내온도에 따라 변화하므로 유입공기의 온도가 17℃일 때는 130W/㎡, 10℃일 때는 170W/㎡을 경계조건으로 입력하였다. 예측한 공기유동의 형태는 실험값(Boon, 1978)과 비교하여 대체로 만족할만한 결과를 얻었다. 그러나 유입공기의 온도가 10℃인 경우, 예측 공기유동은 실험 유동형태와 차이가 있었다. 즉, 실험에서는 수평슬롯으로 유입된 공기가 바로 아래로 굴절되어 流動하였으나, 계산의 결과는 일정 거리로 수평방향으로 유동하다가 아래로 굴절하였다. 이런 유동의 차이는 경험적으로 熱浮力에 민감하게 반응하지 않는 k-ε 亂流모형의 적용이 원인이 되거나 실험의 부적절한 수행이 원인이 될 수도 있다. 이 流動의 Reynolds 數 (Re)는 약 3,300, 修正Ar數(Corrected Archimedes Number ; Ar_c) 64로써, Ar_c <30 이거나 Ar_c> 75이면 유입공기의 제트는 수평유동한다는 Randall & Battams (1979)의 연구결과와는 일치하였다. 그러나 공기제트의 굴절은 유동의 특성이 같다하더라도 유체의 성질, 축사의 기하학적 형태에 따라서 매우 민감하게 반응하므로 실제 실험을 통한 재검정과정을 거쳐야 할 것으로 판단된다. Fig. 9와 Fig. 10의 기하학적 형태의 지점별 예측온도와 측정온도(Boon, 1978)와의 편차는 대부분의 지점에서는 1℃ 미만으로 상당히 정확하였으며, 최대의 온도차는 Fig. 10의 지점 13에서 1.7℃이었다.

---

* This paper was presented in the International Symposium on 「Room Air Convection and Ventilation Effectiveness」 at the University of Tokyo, July 22~24, 1992.

* 慶尙大學校 農科大學 農工學科

I. Introduction

The rapid rise of the value of land and wages has led to the development of a livestock industry which relies on more confined methods of production. Since improper indoor environments lower the efficiency of production and reproduction of animals in a confined livestock building and detrimental to workers (Scott et al., 1983[1] ; Choi, 1989[2]), it is necessary to provide an appropriate indoor environment.

Temperature, humidity, and contaminants (dust and harmful gases) are the major environmental parameters controlled. Mechanical ventilation is a practically acceptable medium to dilute contaminants in a confined livestock building. A conventional ventilation graph based on temperature, humidity and contaminant control was defined by Christianson and Fehr(1983)[3]. This determines the ventilation rate needed assuming complete mixing.

It often happens that incoming air is exhausted to outlet without mixing with existing indoor air(short-circuiting) or that air speeds reach almost zero in some regions(stangnant zone) so that ventilation air flow does not dilute effectively contaminants in a building. Determining the ventilation rate based on the conventional ventilation graphs is necessary but not sufficient. A quantitative study should go along with a qualitative study to confirm the effectiveness of the ventilation system for a livestock building (Albright, 1990)[4]. A qualitative study includes predicting scalars (temperature, humidity and contaminants) distributions determined by air flow in a ventilated building determined by air flow. Thus it is important to explore air flow patterns in a livestock building, which provides basic information for optimum design of the ventilation system.

A research group of NIAE in U.K. has conducted extensive experimental work on air flow patterns in a full-scale livestock building. Carpenter et al. (1972)[5], Randall (1975)[6], Randall and Battams (1976)[7], Boon (1978)[8], Capenter and Moulsely (1978)[9], Randall (1979)[10], Randall (1980)[11], Boon (1984)[12] visualized air flow patterns for various flow configurations in a livestock building ; the effect of building layout, the effect of ambient temperature, and the effect of internal obstruction. Some of their works studied the stability criterion of non-isothermal air flow. However, since the adjustment of the parameters of structure and ventilation system is both difficult and in expensive a full-scale experimental structure, it is not readily adaptable for prediction of air movement in a livestock builiding. This is the major shortcoming of experimental work.

Timmons(1979)[13] employed fluid dynamic theory in simulating air flow in a ventilated space to overcome the limitation of experiment. He formulated the modified inviscid Navier-Stokes equations with the ψ-ω method to simulate overall air flow patterns, which has not been often used due to its serious shortcomings. Choi et al.(1988, 1990)[14,15] applied the k-ε turbulence model for calculation of air velocities in a ventilated enclosure with and without internal obstruction.

The work presented in this article was to investigate the effect of buoyancy force on air flow, created by the difference between the temperature of entering air jet and that of the room, and the effect of obstruction. A modified version of the TEACH-like computer code was used to predict air flow in a ventilated livestock building.

II. Mathermatical Model

1. Turbulence Model (two-equation model : k-ε model)

Since air motion in a livestock building is bascially turbulent flow, the terms created in derivation of the governing equations for turbulent air motion should be quanitified. The oldest proposal for modeling the turbulent stresses, $-\langle uiuj\rangle$ turned out to become a significant part of most turbulence models of practical use today. Boussinesq's eddy-viscosity concept which assumes that, in analogy to the viscous stresses in laminar flows, the turbulent stresses are proportional to the mean-velocity gradients. For general flow situations, this concept may be expressed as :

$$-\langle u_i u_j\rangle = -\nu_t\left(\frac{\partial U_i}{\partial x_j}+\frac{\partial U_j}{\partial x_i}\right)-2/3k\ \delta_{ij}\cdots(1)$$

Turbulent viscosity(ν_t), in contrast to the molecular viscosity(ν), is not a fluid property but depends strongly on the state of turbulence. Turbulence is assumed to be characterized by the turbulent kinetic energy, k, and its dissipation rate, ε, known as the two-equation turbulence model. Turbulent viscosity is determined by local values of k and ε.

$$\nu_t = C_\mu \frac{k^2}{\varepsilon} \cdots\cdots (2)$$

2. Grid Generation for Curvilinear Coordinates

In general, grid generation is a mapping between a physical space and a computational space(see Fig. 1). The transformation is given by the functions[16] :

$$\xi=\xi(x,\ y) \cdots\cdots (3a)$$
$$\eta=\eta(x,\ y) \cdots\cdots (3b)$$

obian(J) can be defined in Eq.(4) and ξ_x, ξ_y, η_x, η_y can be exptessed in terms of J. Note that ξ_x denotes $\partial\xi/\partial x$, η_x denotes $\partial\eta/\partial x$.

$$J=(x_\xi,\ y_\eta - x_\eta\ Y_\xi)=(\xi_x\ \eta_y-\xi_y\ \eta_x)^{-1} \cdots\cdots (4)$$
$$\xi_x=y_\eta/J\ ;\ \xi_y=-x_\eta/J\ ;\ \eta_x=-y_\xi/J\ ;\ \eta_y=x_\xi/J \cdots\cdots (5)$$

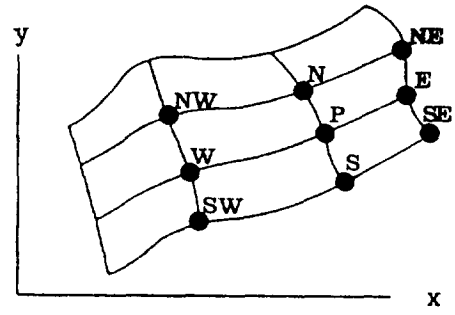

a. Physical Plane

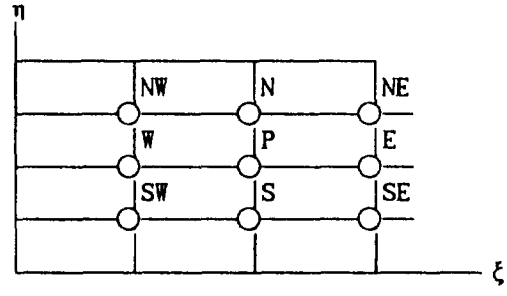

b. Computational Plane

Fig. 1 Mapping from physical plane to computational plane

3. Governing Equations

Air motion in a livestock building is bascially a turbulent flow, which is governed by the laws of mass, momentum, and energy conservation. The governing differential equations of turbu-

lent flow take the following forms for steady-state, two dimensional, non-isothermal mean flow. The equations are expressed by the Curvilinear Coordinates.

1) Continuity :

$$u_x + v_y = 0 \quad \cdots\cdots (6)$$

$$\rightarrow \{\{J(\xi_x u + \xi_y v)_\xi\} + \{J(\eta_x u + \eta_y v)_\eta\}/J = 0 \quad \cdots\cdots (7)$$

The inverse-tranformation vectors, U and V can be defined in terms of velocities in x-direction, u, and velocity in y-direction, v, in Cartesian Coordinates. U and V are a velocity component perpendicular to ξ, η, respectively.

$$U = \xi_x u + \xi_y v : \quad V = \eta_x u + \eta_y v \quad \cdots\cdots (8)$$

2) U-Momentum Transport Equation :

$$u_t + (uu)_x + (uv)_y = -p_x + (2 \nu_t u_x)_x + (\nu_t (u_y + v_x))_y \quad \cdots\cdots (9)$$

$$\rightarrow Ju_t + (JUu)_\xi + (JVu)_\eta = -(J\xi_x p)_\xi - (J\eta_x p)_\eta + (J\nu_t((2\xi_x^2 + \xi_y^2)u_\xi + (2\xi_x\eta_x + \xi_y\eta_y)u_\eta + \xi_x\xi_{-y}v_\xi + \xi_y\eta_x v_\eta))_\xi + (J\nu_t((2\eta_x\xi_x + \eta_y\xi_y)u_\xi + (2\eta_x^2 + \eta_y^2)u_\eta + \eta_y\xi_x v_\xi + \eta_x\eta_y v_\eta))_\eta \quad \cdots\cdots (10)$$

3) V-Momentum Equation :

$$v_t + (uv)_x + (vv)_y = -p_y + (\nu_t(u_y + v_x))_x + (2\nu_t v_y)_y \quad \cdots\cdots (11)$$

$$\rightarrow Jv_t + (JUv)_\xi + (JV_v)_\eta = -(J\xi_y p)_\xi - (J\eta_y p)_\eta + (J\nu_t((\xi_x^2 + 2\xi_y^2) v_\xi + (\xi_x\eta_x + 2\xi_y\eta_y) v_\eta + \xi_x\xi_y u_\xi + \xi_x\eta_y u_\eta))_\xi + (J\nu_t((\eta_x\xi_x + 2\eta_y\xi_y)v_\xi + (\eta_x^2 + 2\eta_y^2)v_\eta + \eta_x\xi_y u_\xi + \eta_x\eta_{-y}u_\eta))_\eta \quad \cdots\cdots (12)$$

4) Turbulent Kinetic Energy Transport Equation (k) :

$$k_t + (ku)_x + (kv)_y = (\nu_t k_x/\sigma_1)_x + (\nu_t k_y/\sigma_1)_y + \nu_t S - \varepsilon \quad \cdots\cdots (13)$$

$$\rightarrow Jk_t + (JUk)_\xi + (JVk)_\eta = (J\nu_t((\xi_x^2 + \xi_y^2) k_\xi + (\xi_x\eta_x + \xi_y\eta_y)k_\eta)/\sigma_1)_\xi + (J\nu_t((\xi_x\eta_x + \xi_y\eta_y)k_\xi + (\eta_x^2 + \eta_y^2)k_\eta)/\sigma_1)_\eta + J\nu_t S - J\varepsilon \quad \cdots\cdots (14)$$

where, $S = 2u_x^2 + 2v_y^2 + (u_x + v_y)^2$

$$S = 2(((J\xi_x u)_\xi + (J\eta_x u)_\eta)/J)^2 + 2(((J\xi_y v)_\xi + (J\eta_y v)_\eta)/J)^2 + (((J\xi_y u + J\xi_x v)_\xi + (J\eta_y u + J\eta_x v)_\eta)/J)^2$$

5) Dissipation rate of Turbulent Kinetic Energy Transport Equation (ε-equation) :

$$\varepsilon_t + (\varepsilon u)_x + (\varepsilon v)_y = (\nu_t \varepsilon_x/\sigma_2)_y + (\nu_t \varepsilon_y/\sigma_2)_y + c_1\varepsilon\nu_t S/K - c_2 \varepsilon^2/k \quad \cdots\cdots (15)$$

$$\rightarrow J\varepsilon_t + (JU\varepsilon)_\xi + (JV\varepsilon)_\eta = (J\nu_t((\xi_x^2 + \xi_y^2)\varepsilon_\xi + (\xi_x\eta_x + \xi_y\eta_y)\varepsilon_\eta\}/\sigma_2)_\xi + (J\nu_t((\xi_x\eta_x + \xi_y\eta_y)\varepsilon_\xi + (\eta_x^2 + \eta_y^2)\varepsilon_\eta)/\sigma_2)_\eta + Jc_1\varepsilon\nu_t S/k - Jc_2\varepsilon^2/k \quad \cdots\cdots (16)$$

6) Thermal Energy Transport Equation (h) :

$$h_t + (hu)_x + (hv)_y = (\gamma_t hx/\sigma_1)_x + (\gamma_t hy/\sigma_1)_y \quad \cdots\cdots (17)$$

$$\rightarrow Jh_t + (JUh)_\xi + (JVh)_\eta = (J\gamma_t((\xi_x^2 + \xi_y^2) h_\xi + (\xi_x\eta_x + \xi_y\eta_y) h_\eta)/\sigma_1)_\xi + (J\gamma_t((\xi_x\eta_x + \xi_y\eta_y) h_\xi + (\eta_x^2 + \eta_y^2) h_\eta)/\sigma_1)_\eta \quad \cdots\cdots (18)$$

where, $\gamma_t = \nu_t/Pr_t$

Table 1. Value of Constants in the Eq.(8)~(18)

C_u	C_D	C_1	C_2	σ_1	σ_2
0.09	1.0	1.44	1.92	1.0	1.3

Ⅲ. Numerical Analysis

1. Discretization by the Control Volume Methods

Eq.s (6)~(18) can be expressed in the discretized equations for single phase flow. Non-staggered grid and QUICK scheme were applied not only to scalar transport equations but

also to momentum transport equations to formulate discretized equations in the curvilinear coordinates.

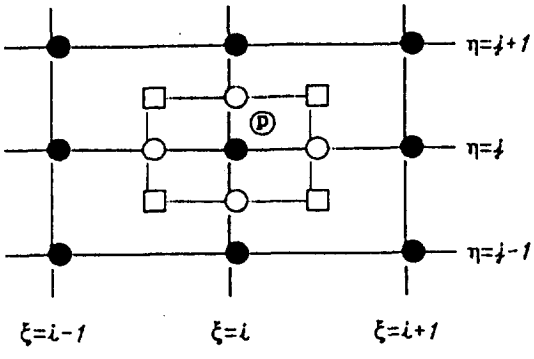

a. Grids for a Full Control Volume

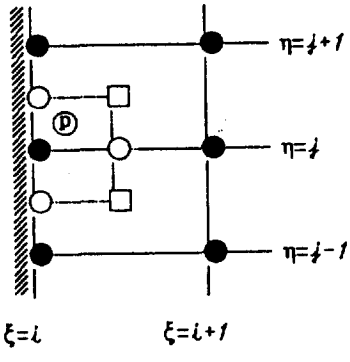

b. Grids for a Half-Control Volume at Walls

Fig. 2 Computational Control Volume for Integration

The discretized equations were obtained by integrating the governing equations at the control volume in Fig. 2a in which all dependent variables are defined at the same nodal point, Ⓟ. The convective, the diffusive, and pressure gradient terms of the governing equations take the identical form of Eq.(19).

$$F=(R_\xi+S_\eta)/J \quad \cdots\cdots (19)$$

$$\int_\omega F d\omega=\int_{j-1/2}^{j+1/2}\int_{i-1/2}^{i+1/2} F\,J\,d\xi d\eta=\int_{j-1/2}^{j+1/2}\int_{i-1/2}^{i+1/2}(R_\xi+S_\eta)d\xi d\eta=R(i+1/2,\ j)-R(i-1/2,\ j)+S(i,\ j+1/2)-S(i,\ j-1/2) \quad \cdots\cdots (20)$$

The discretized equation at walls was obtained by integrating Eq.(19) at a half control volume for nodal point Ⓟ :

$$\int_\omega F d\omega=R(i+1/2,\ j)-R(i,\ j)+(S(i,\ j+1/2)-S(i,\ j-1/2))/2 \quad \cdots\cdots (21)$$

The integrating area can be changed similarly for the one-fourth or the one-eight control volume types according to the location of control volume. An integration for a term that cannot be expressed in the form of the surface integration represents the value at the nodal point, ie., a value at the center of the control volume. For example, the integration of the production term of the k transport equation (14) can be expressed as follows :

$$\int_\omega \nu_\tau\, Sd\omega=\int_{j-1/2}^{j+1/2}\int_{i-1/2}^{i+1/2}\nu_\tau\, S\,J\,d\xi d\eta=(J\nu_\tau\ S)_{ij} \quad \cdots\cdots (22)$$

An algebraic equation of discrete dependent variables can be obtained at each nodal point by integration over the cooresponding control volume with Eq.s (19) and (20).

These algebraic equations can be solved at all nodal points simultaneously using a relaxation method.

2. QUICK Scheme

The Quick scheme was applied to formulate the convection term of momentum equations (Leonard, 1980)[17] and the transport equations of k and ε in this study. When expressing the convection term in a form of Eq.(19), the terms, R(i+1/2, j), R(i−1/2, j) in Eq.(20) mean momentum flux through the surface with constant ξ, which can be expressed by :

$R(i-1/2,\quad j)=((JU)_{i-1/2,j}\{((u_{i,j}+u_{i-1,j})/2-CURVN/8+CURVT/24\}$ ····· (23)

where, CURVN/8 and CURVT/24 shows upwind effect in discretization.

if $U_{i-1/2,j}>0$, then $CURVN=u_{i,j}-2u_{i-1,j}+u_{i-2,j}$; $CURVT=u_{i-1,j-1}-2u_{i-1,j}+u_{i-1,j+1}$ ····· (24)

if $U_{i-1/2,j}>0$, then $CURVN=u_{i+1,j}-2u_{i,j}+u_{i-1,j}$; $CURVT=u_{i,j-1}-2u_{i,j}+u_{i,j+1}$ ····· (25)

3. Boundary Conditions

In a curvilinear coordinate system, the boundary surface is treated as a curved surface with a constant value of ξ, η, regardless of its complexity. Such a property makes the computational boundary easy to formulate the boundary conditions.

In the present method, the imaginary computational boundary is set just inside the physical region of the flow field. The computational boundary surafce is parallel to the physical boundary surface apart from the short distance, △H, shown in Fig. 3. Thus, small deviation of surface area between the physical boundary and the computational boundary was ignored in the computation. With this positioning of the boundary,

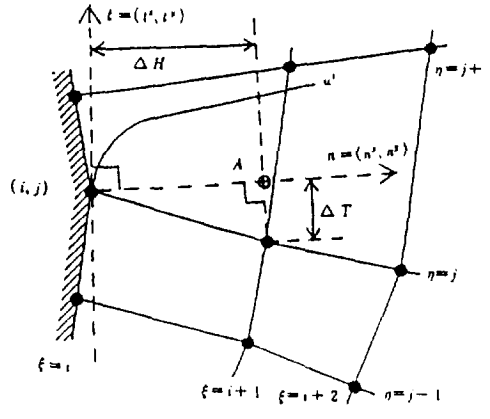

Fig. 3 Velocity components at wall boundary

velocity components at the computational boundary, as well as those within the inner flow region may be calculated using momentum equations. The physical boundary imposes its boundary conditions on the computational boundary, which is set just inside the physical surface, using the proper wall law or wall function.

Wall boundary conditions for velocity components, turbulent kinetic energy, and its dissipation rate were based on power law, free slip condition, and wall function respectively. More details about boundary conditions are found in Patankar(1980)[18].

1) boundary conditions for velocity components (power law) :

$u^t=U^{II}(N/\triangle H)^m$ ····· (26)

where, $U^{II}=u^t_{i+1,j}+\{\partial u^t/\partial T\}\triangle T\rightarrow u^t_{i+1,j}+[\{u^t_\xi(\xi_x,\xi_y)+u^t_\eta(\eta_x,\eta_y)\}_{i+1,j}\cdot(t^x,t^y)]\triangle T$

$\triangle H=(x_\xi, y_\xi)-(n^x, n^y)$

$\triangle T=-(x_\xi, y_\xi)-(t^x, t^y)$

2) boundary conditions for turbulent kinetic energy(free slip condition) :

$\partial k/\partial N=(\xi_x,\xi_y)\cdot(n^x,n^y)k_\xi+(\eta_x,\eta_y)_{ij}\cdot(n^x,n^y)k_\eta=0$ ····· (27)

where, $k_{ij}=k_{i-1,j}+\gamma(k_{ij-1}-k_{ij-1})/2$

$\gamma=((\eta_x,\eta_y)_{ij}\cdot(n^x,n^y))/((\xi_x,\xi_y)_{ij}\cdot(n^x,n^y))$: aspect ration

3) boundary condition for dissipation rate (wall function) :

$\partial\varepsilon/\partial N=(\xi_x,\xi_y)_{ij}\cdot(n^x,n^y)\varepsilon_\xi+(\eta_x,\eta_y)_{ij}\cdot(n^x,n^y)\varepsilon_\eta=(\varepsilon^h-\varepsilon_{ij})/h$ ····· (28)

where, $\varepsilon^h=((C_D{}^{3/4})/xh)\ k_{ij}{}^{3/2}$

$\varepsilon_{ij}=(\varepsilon_{i+1,j}/\triangle H-\varepsilon^h/h+(\eta_x,\eta_y)_{ij}\cdot(n^x,n^y)(\varepsilon_{ij-1}-\varepsilon_{ij-1})\}/(1/\triangle H-1/h)$

4. SIMPLE-like Algorithm

The solution algorithm is a marching one,

that sweeps the domain in a slab-by-slab fashion. A slab is an X-Y plane of cells, and contains NX * NY cells. The code has three levels of iteration. The iteration level 1 in Fig. 2 the NX * NY system of equations for a variable ϕ at each slab, using either a generalized 2D version of the well-known Tri-Diagonal Matrix Algorithm (TDMA) or a Jacobi point by point procedure. The iteration level 2 has to blend together the changes effected for each variable separately. The pressure/velocity linkage has also to be dealt with this level. The pressure field has to be such that the velocities resulting from the momentum equations verify the continuity equation.

The iteration level 3 repeatedly solve the equations for all variables including pressure correction updating the corrections between them. In the slab by slab procedure, the off-slab values are assumed known, whereas they are not. As a consequence, the solution for the current slab is not the final one, and the solution procedure has to sweep all the slab in the domain several level. A more detailed dicussion of SIMPLE-like Algorithm was given by Patankar (1980)[18].

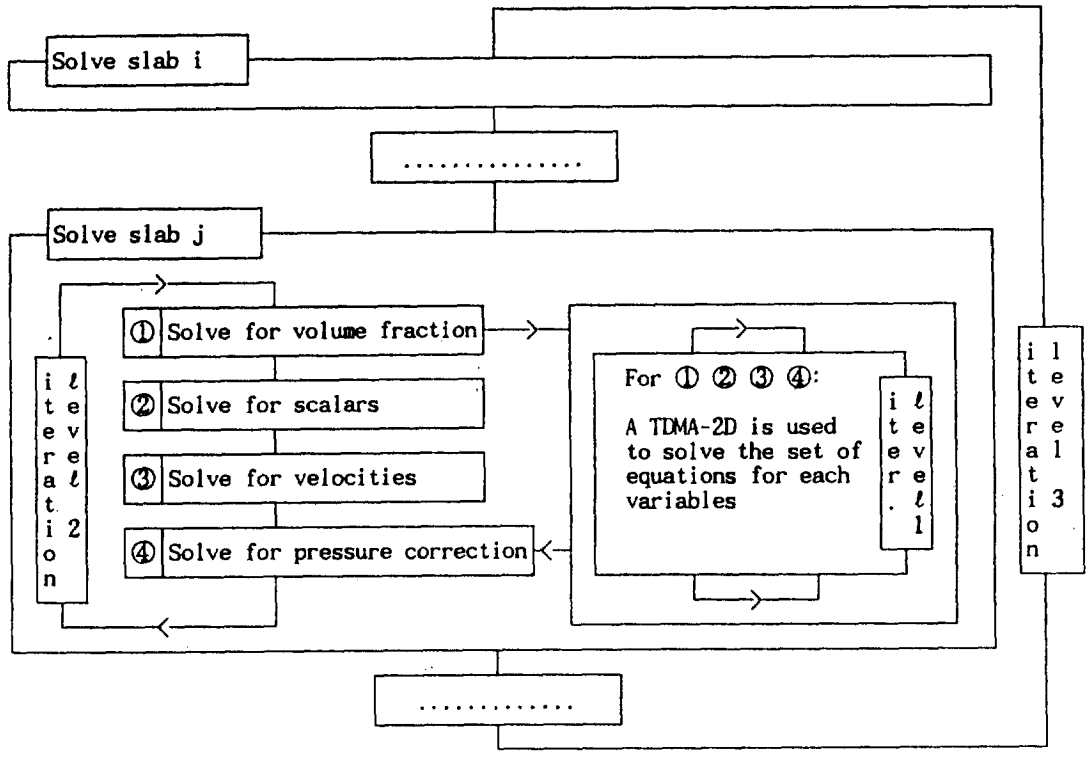

Fig. 4 Solution algorithm for two dimensional discretized equations.

Ⅳ. Result and Discussion

Air flow patterns for geometries of Fig. 6a~ Fig. 7b were visualized by Boon(1978), using liquid film bubbles in the flow, and were utilized to examine the capability of the simulation model applied in predicting a realistic air flow.

1. Experimetal Procedure

The full-scale section of a livestock building used for calculation geometry, Fig. 5 in this work was described in detail in Boon(1978). The section was 7.80 m wide representing a typical span which may accomodate two pig pens and three passages. It was arranged with solid walls, 1.05 m high, to form a feeding passage at each side and with a central wall to form two pens. The cross-section of the experimental livestock building is shown in Fig. 6 with the presence, and Fig. 7 with the absence of solid walls. The depth of the section represented the length of one pen and the height was 1.87m to the eaves and 2.43m to the ridge. An insulated shell connected to an air conditioner and enclosing the side walls and roof allowed the temperature outside the section to be controlled. Ventilating air was exhausted from the shell by a 0.46m propeller fan was mounted 0.45m above the ceiling in a vertial duct. Heat released from the stock resulted from 26 large white pigs, 13 in each pen, generating heat 170 W/m² for 10℃, 130 W/m² for 17℃. The air inlet was a 0.04m wide slot, the full length of the building section, near the top of each side wall 1.70m from the floor. Approximately 0.52m³/s for inlet air temperature of 17℃ and 0.16m³/s for 10℃. The outlet was 0.52 m² aperture in the center of the apex of the roof.

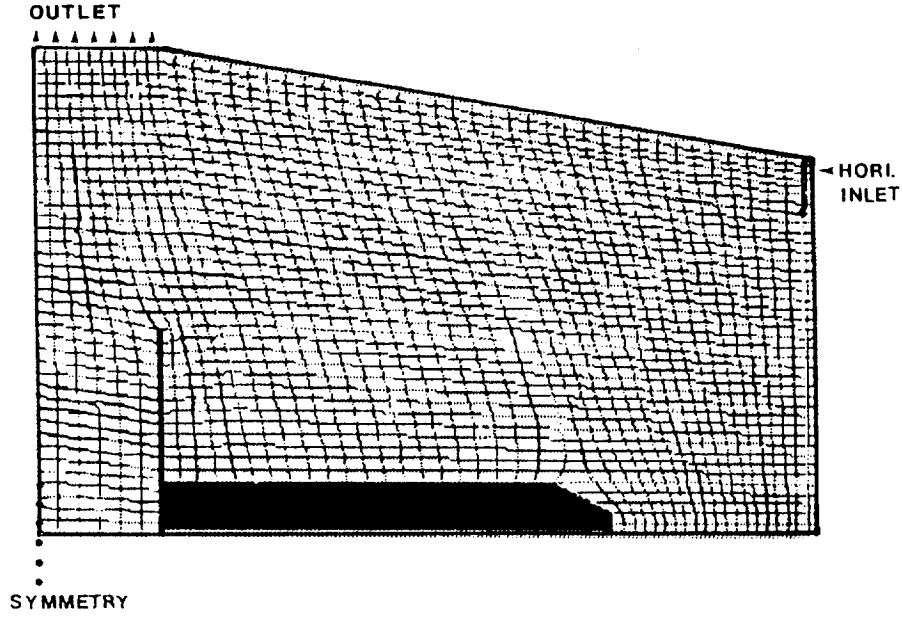

Fig. 5 Calculation Domain with Curvilinear Coordinate system

2. Air Flow Patterns

1) The Effect of Obstruction

The inlet air jet enters horizontally in flow configurations of Fig. 6 and Fig. 7 with the entering air temperature of 17℃ and its velocity of 3.84m/s (Reynolds number of 1E+4). The only difference in the flow configurations is the presence of physical obstruction. Overall similarities were perceived between the calculated and the observed air flow in Fig. 6 and Fig. 7. No distinct difference of air motion is observed in Fig. 6a and in Fig. 7a either with or without internal obstacles. There is, however, a difference in the size of a primary recirculation flow. Boon's observation do not show the details of air motion and the magnitude of air velocities, but calculations in this work, reveal such details Fig. 6b and Fig. 7b. The more detailed air motion in this work provides additional information.

The calculated air flow of Fig. 6b with the presence of an obstacle shows primary recirculation in the center of the space : it rotates counterclockwise and is squeezed due to the solid wall. A seconadry recirculation flow is observed between the symmertric line and the internal solid wall, which separates the passage and the pig pen. Initially a free air jet in Fig. 6b deflects upwards and attaches to the ceiling due to Coanda effect. The reattached flow becomes a wall jet and continues to move along the ceiling. The solid wall creates a dominating adverse pressure gradient, which leads to flow separartion. A weak eddy is also observed in the lower right corner of Fig. 6b.

The physical obstructions in Fig. 6 modifies air flow significantly. They deflect air flow and lead to flow separations by creating an adverse pressure gradient, and dissipate the turbulent kinetic energy of the air flow. In most cases, physical obstructions disrupt the internal air flow. However, they purposefully were utilized to redirect or to decelerate air flow. As shown in Fig. 6b, air velocities are relatively smaller, compared to those of Fig. 7b. In paricular, the air velocities approaches zero at the height of animals while those in other regions have larger velocities. Except cold winter, it is desirable to have higher air velocities to maintain proper indoor thermal and chemical environments.

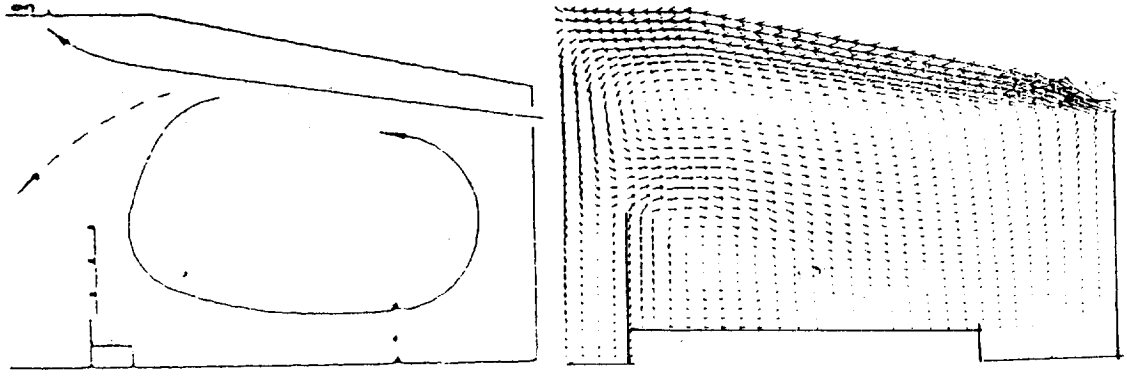

(a) (b)

Fig. 6 a) the observed by Boon(1978)
b) the calculated flow patterns

A short-circuiting phenomenum is observed in the flow configuration of Fig. 6 and Fig. 7. Much of the entering air flow through the slot inlet at eave is exhausted by the fan at the ridge. A recirculating air forms a primary flow with lower velocity, so with lower momentum, rotates counterclockwise, and it again separates at the top of the internal solid wall. Some of air is entrained by the inlet air jet, and the rest forms the secondary eddy rotating clockwise in the region between the internal solid wall and the inlet wall. Basically, air flow with less momentum has less ability in diluting contaminants. Excessive harmful gases or dust may accumlulate on the pigs or on the floor since the overall velocity is much smaller in the flow field.

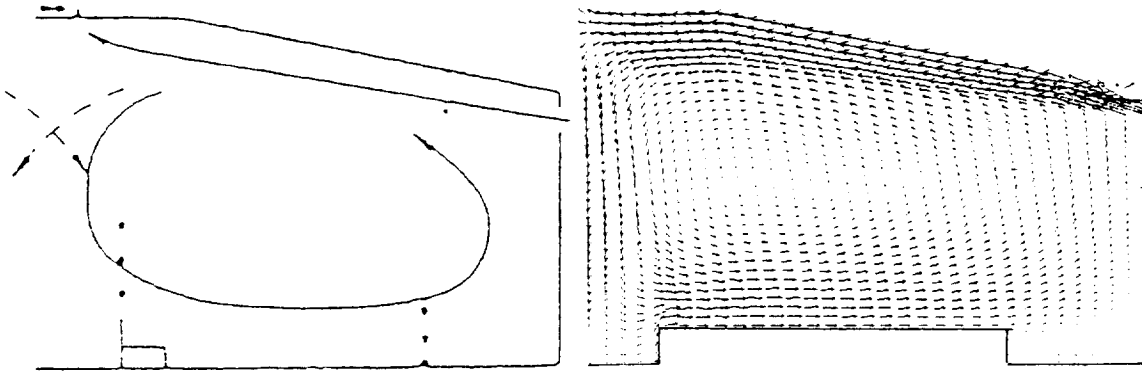

(a) (b)

Fig. 7 a) the observed by Boon(1978)
b) the calculated flow patterns

2) The Effect of Ambient Temperature

To see the effect of thermal buoyancy force on air flow, the entering air temperature of 10℃ was applied to the flow geometry of Fig. 6 with heat flux of 170 W/㎡, released from real pigs at floor.

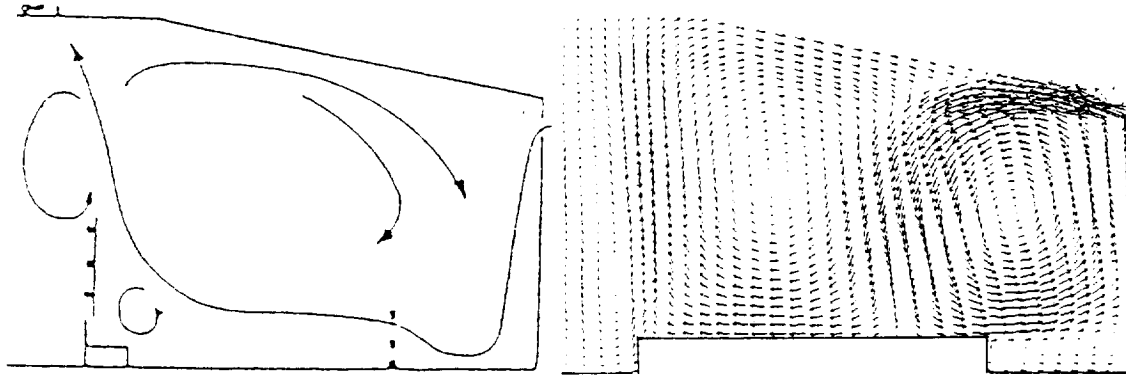

(a) (b)

Fig. 8 a) the observed by Boon(1978)
b) the calculated flow patterns

The calculated air flow in Fig. 8b moves forwards, and falls down in the middle of the space and rotates clockwise. This may indicate that that buoyancy force overcomes inertia force. However, the observed air flow in Fig. 8a falls down immediately after entering, and rotates counter-clockwise. According to experience, perhaps discrepancy of the observed in Fig. 8a and the calculated air flow in Fig. 8b originated from the insensitivity of the k−ε turbulence model itself to buoyancy, or from improper management of experiment. Since the flow is turbulent, the buoyancy may overcome inertia force at some distance from the inlet.

The inlet corrected Archimedes Number (Ar_c) was used to identify the ventilating conditions for this non-isothermal arrangement, defined by Randall (1979)[10].

$$Ar_c=\frac{C_d g A_s WH(W+H)(T_s-T_i)}{Q^2(546+T_s+T_i)} \quad \cdots (29)$$

The Ar_c in Eq. (29) characterize the ratio of the buoyancy and the inertia force which determines the air flow pattern. They concluded that the jet remains horizontal if $Ar_c<30$ and falls if $Ar_c>75$. For this study, the Ar_c was about 64 which was in the range of unstable flow. The calculated air flow pattern of Fig. 8b was supported by the work of Randall(1979), however, it jeopardizes the observation by Boon(1978) in Fig. 8a. Further study may be necessary to ensure the cause of such discrepancy. The unstable air flow shown in Fig. 8b, if it should be true, may create a chilly draft to the animals. In case, it is recommended to direct entering air jet downwards so that the cold jet gets warmer along the inside wall.

2. Air Temperature Distribution

Fig. 9 and Fig. 10 show comparisons of the measured air temperatures and the calculated over the space for the flow configurations of Fig. 6 and Fig. 7 respectively, in order to validate the simulation. The calculated air temperatures deviated less than 1℃ from the measured for the flow configuration of Fig. 6. The maximum temperature difference between two was only 0.6℃ at the center passage between the solid pen fronts at central passage (Pts. 4, 5) and just above the right end of stock near the east wall (Pt. 13). The calculated temperatures were in excellent agreement with measurements. It is interesting, however, to note that the points of maximum temperature difference located in the lower velocity region (stagnant region). Since air flow determines temperature distribution over the space, relatively less accurate prediction of air flow at that region may lead to the maximum difference. Thermal accumlations are observed at the upper-left region of the stock (obstruction) and the right end of the stock in Fig. 9 due to flow separation by physical obstacles.

The deviation of the calculated air temperatures from the measured for the flow configuration of Fig. 6 was about 1℃. The maximum temperature difference between two was 1.7℃ at Pt. 13. Thermal accumlations was observed at the upper-right region of the stock (obstruction) in Fig. 10 due to continuous heat flux from stock and direction of primary recirculating air flow rotates counter-clockwise. The calculated air temperatures, in general, were in good agreement with measurements. Considering the validity of the two calculated temperature fields with measurements shown in Fig. 9 and Fig. 10,

computer simulation can be used to obtain basic information for design of ventilation system.

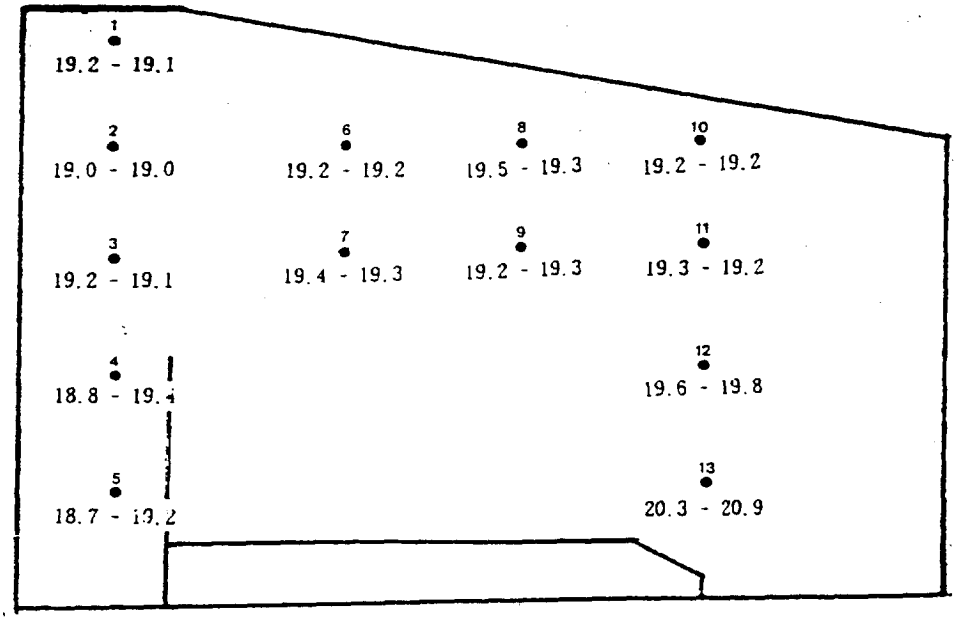

Fig. 9 Comparison of the measured by Boon (1978) and the calculated spatial temperature for flow configuration of Fig. 6

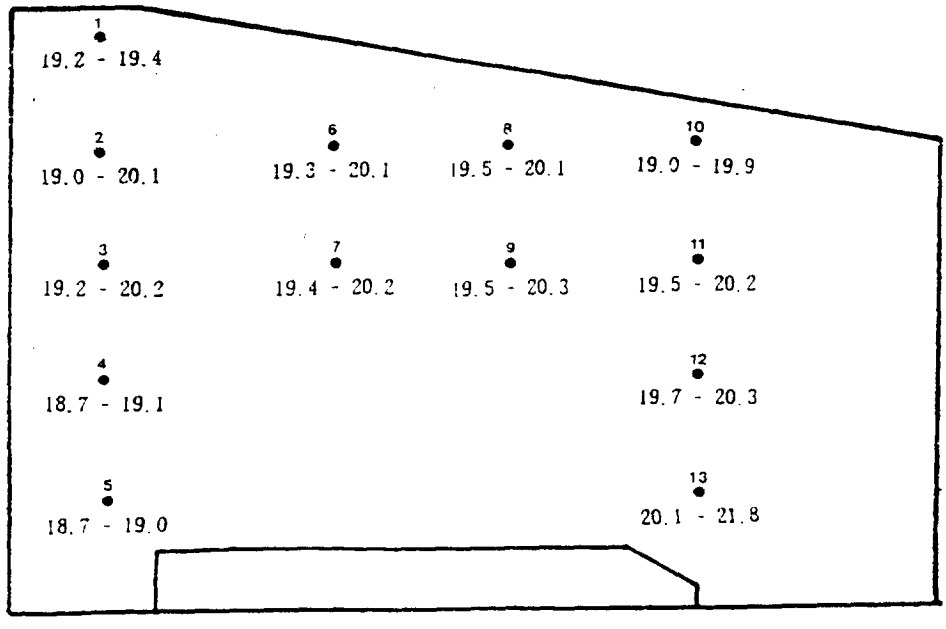

Fig. 10 Comparison of the measured by Boon (1978) and the calculated spatial temperature for flow configuration of Fig. 7

V. Conclusion

The TEACH-like program, which uses the k-ε turbulence model, was applied to a ventilated air space having obstructions : 26 real pigs with heat flux of 130 W/㎡ for inlet temperature of 17 ℃ and Reynolds number of 1E+4, and 170W/㎡ for 10℃ and Re of 3E+3. Results were compared to experimental data and the following conclusions were drawn.

1. It is possible to predict, with good accuarcy, overall flow patterns and temperature distributions in a ventilated space, representing a typical livestock building having physical obstructions, by solving discretized conservation equations and using the standard k-ε model.

2. Physical obstruction in a ventilated space significantly modifies air flow and/or creates stagnant regions where heat accumulates shown in Fig. 5b. Since air velocities are the order of 1E-2 at stock level, contaminants produced by animals can not be properly diluted by such ventilation system. Carefully examination of air velocities and temperatures should be carried out at stock level.

3. The horizontally directed unstable air flow, deterimental to animals in cold weather, can be avioded by directing entering air jet to downwards.

4. It is recommended to simulate air flow and temperature distributions in a ventilated space for design purpose to evaluate the efficiency of the ventilation system to be installed.

Nomenclature

x, y : physical coordinates
ξ, η : Computational coordinates
u, v : velocities in x, y-direction
U, V: inverse-transformation vector of u, v
p : modified static pressure(=(static pressure+2/3k)/ρ)
k : turbulent kinetic energy
h : enthalpy
S : source term
T_s : surface temperature of the simulated pigs [℃]
T_i : inlet air temperature [℃]
P_{rt} : turbulent Prandtle number
α : thermal diffusivity
ε : energy dissipation
ν_t : turbulent viscosity
φ : varaibles in question

〈sub-or superscripts〉

ϕ_{ij} : discretized equation at node of ξ =i, η=j
ϕ_x, ϕ_y, ϕ_t : partial derivatives with respect to x, y, t
ϕ_ξ, ϕ_η : partial derivatives of ξ, η
ϕ^l : components of tangential direction
ϕ^x, ϕ^y : components of x, y direction
σ_t : turbulent Prandtl number
l : laminar
t : turbulent

References

1. Scott N.R., J.A. DeShazer, and W.L. Hellickson. 1983. Chapter 7. Effects of the thermal and gaseous environment on livestock. in M. A. Hellickson and J.N. Walker(editors). Ventilation of Agricultural Structures. ASAE Monograph No.6. St. Joseph, MI.
2. Choi, Hong-Lim. 1989. Ventilation of Agricultural Structures. Daegwang Pub.
3. Christianson L.L. and R.L. Fehr. 1983. Chapter 14. Ventilation-Energy and Economics in Hellickson M.A. and J.N. Walker(editors) Ventilation of Agricultural Structures. ASAE Monograph No.6. St. Joseph, MI.
4. Albright L.D. 1990. Environments Control for Animals and Plants, Am. Soc. Agric. Engrs, St.Joseph, MI.
5. Carpenter, G.A., L.J. Mousley and J.M. Randall. 1972. Ventilation investigation using a section of a livestock building and air flow visualization by bubbles. JAER Vol. 17 No.4, pp. 323－331.
6. Randall, J.M. 1975. The prediction of air flow patterns in a livestock building. JAER Vol. 20, No. 2, pp. 199－215.
7. Randall, J.M and V.A. Battams. 1976. The observed influence of surface obstructions on the airflow pattern within livestock building. JAER Vol. 21, No. 1, pp. 33－39.
8. Carpenter, G.A. and L.J. Mousley. 1978. Resistance to airflow of materials used in ventilating livestock buildings. JAER Vol. 23, pp. 441－451.
9. Boon, C.R. 1978. Airflow patterns and temperature distribution in an experimental piggery. JAER Vol. 23, pp. 129－139.
10. Randall, J.M. 1979. The stability criteria for airflow patterns in livestock buildings. JAER Vol. 24, pp. 361－374.
11. Randall, J.M. 1980. Selection of piggery ventilation systems and penning layouts based on the cooling effects of air speed and temperature. JAER Vol. 25, pp. 169－187.
12. Boon, C.R. 1984. The control of Climate Environment for finishing pigs using lower critical temperature. JAER Vol. 29, pp. 295－303.
13. Timmons, M.B. 1979. Experimental and numerical study of air movement in slot-ventilated enclosures. Unpublished Ph.D. Thesis, Cornell University.
14. Choi, Hong-Lim, L.D. Albright, M.B. Timmons and Z. Warhaft. 1988. An Application of the k-ε turbulence model to predict air distribution in a slot－ventilated enclosure. Transaction. ASAE Vol 31, No. 6, pp.1804－1814.
15. Choi, Hong-Lim Choi, L.D. Albright and M. B. Timmons. 1990. An Application of the k-ε turbulence model to predict how a rectangular opbstacle in a slot-ventilated enclosure affects air flow. Transaction. ASAE Vol. 33, No. 1, pp. 274－281.
16. Leonard B.P. 1980. The QUICK Algorithm : A uniformly 3rd order finite difference method for highly convective flows. Computer Methods in Fluids, pp. 159～195 Pentech Press.
17. Majundar S. 1986. Development of a finite volume procedure for prediction of fluid flow problems with complex irregular boundaries. Report SFB 210/T/29, University of Karlsruhe.
18. Patankar, P.V. 1980. Numerical Heat Transfer and Fluid Flow. McGraw-Hill Book Company. NY.